Macromolecules

pubs.acs.org/Macromolecules Article

Direct Visualization of Polymerization-Induced Self-Assembly of Amphiphilic Copolymers

Vahid Jabbari, Abhijit H. Phakatkar, Azadeh Amiri, Alireza Ghorbani, and Reza Shahbazian-Yassar*

Cite This: *Macromolecules* 2023, 56, 3171−3182 Read Online

ACCESS | Metrics & More | Article Recommendations | Supporting Information

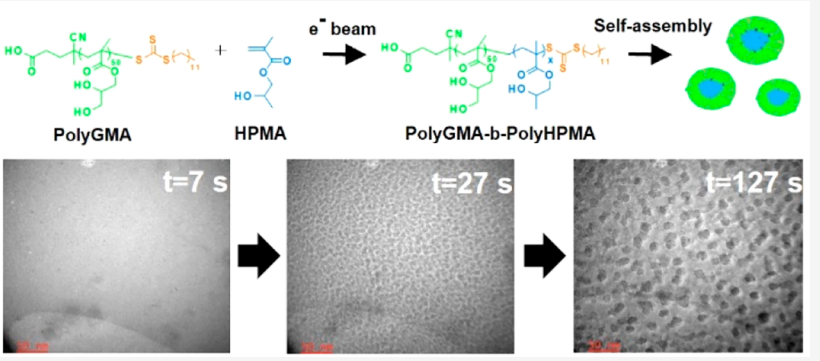

ABSTRACT: The ability to have precise control over the designed structure and properties of molecular self-assemblies is critical for tailoring the quality and efficacy of their functionality, yet the underlying mechanisms governing the evolution from molecules into self-assembled structures are not fully resolved. Here, we employed the graphene liquid cell (GLC) transmission electron microscopy (TEM) approach to observe nucleation and evolution of individual nanoscale micelles during polymerization-induced self-assembly. We speculate that the electron beam induces radical formation by homolytic cleavage of the poly(glycerol methacrylate)−thiocarbonylthio (PolyGMA−thiocarbonylthio) macro-chain-transfer agent (macroCTA), at which it initiates the polymerization of HPMA monomer in aqueous solution. Chain growth of the hydrophobic block, PolyHPMA, and subsequent instability of the resulting block copolymer in the solution trigger the formation of the nanoscale polymer self-assemblies. The spinodal decomposing mechanism is proposed here for the formation and evolution of the polymer assemblies. Such in-situ visualization of polymeric micelle formation, devoid of metal-ion labeling, provides new insights into understanding the complex mechanism of the self-assembly process in amphiphilic molecules.

1. INTRODUCTION

Molecular self-assembly is a pervasive occurrence in biological systems that is responsible for formation of functional structures (e.g., molecular cluster, tubes, helices, and ribbons) from nanoscale to macroscale dimensions. The structure is controlled by a physical or chemical stimulus such as hydrogen bonding, electrostatic forces, dipole−dipole interactions, $\pi-\pi$ stacking, and hydrophobic forces.[1−4] Important examples of self-assembled biological systems include cell membranes, folded proteins, transport vehicles, and reaction vessels with controlled composition and size. During the past years, much attention was paid to implement this bio-inspired strategy in synthetic systems that possess higher physical and chemical flexibility to develop new materials and devices.[5−8] In the synthetic systems, block copolymers, phospholipids, and surfactants form various amphiphilic assemblies such as toroidal structures, micelles, and vesicles, with applications in biomedicine, catalysis, separation science, food science, and templated synthesis.[9,10] To design particular structures with precise control often observed in natural systems, knowledge of the kinetic and thermodynamic landscapes of the self-assembly process is essential. Despite much efforts, the mechanism of the molecule-to-assembly transition in amphiphilic systems is still not entirely resolved.[11−14]

Transmission electron microscopy (TEM) can visualize morphological and structural properties of soft matter and hard matter at the nanoscale and atomic level. Therefore, this technique has been widely used to visualize conventional self-assembly of amphiphilic block copolymers by direct dissolution of the copolymer in a selective solvent.[15−17] Cai et al.[15] employed polymerization-induced self-assembly to synthesize nanostructured polymeric materials with different morphologies using poly(dimethylaminoethyl methacrylate-*co*-styrene)

Received: November 16, 2022
Revised: March 11, 2023
Published: April 11, 2023

https://doi.org/10.1021/acs.macromol.2c02318
Macromolecules 2023, 56, 3171−3182

(PDMAEMADBT-*co*-St) diblock copolymer. By changing the styrene concentration in the feed and reaction conditions, a variety of morphologies such as spherical micelles, nanostrings, and vesicles were observed. Similar studies have been reported for other block copolymers such as poly(acrylic acid)-*b*-polystyrene (PAA-*b*-PSt), poly(4-vinylpyridine)-*b*-polystyrene (P4VP-*b*-PSt), and poly(ethylene oxide)-*co*-polycaprolactone (PEO-*b*-PCL), in solutions under different application conditions, such as conversion rate of the comonomer, monomer feed molar ratio, and solvent quantity.[11−15,17−19] However, visualization of the molecular self-assembly by dry-state TEM is limited to direct dissolution of the ex-situ synthesized copolymer in a selective solvent.

Direct real-time visualization of nucleation and evolution of polymer structures as they assemble from growing copolymer amphiphiles can offer new insights into the field of molecular self-assembly. For instance, established theories for polymer aggregation, morphological evolution, and reorganization can be examined. Liquid phase transmission electron microscopy (LP-TEM) is an emerging technique for observing evolution and dynamics of materials in liquids, with the vast majority of the studies being on hard/inorganic matter.[20−23] Lately, LP-TEM has been used to study imaging single polymer chains,[18,24,25] observing real-time polymerization and reactions initiation and particles growth,[20,23,26−30] observing micellization or vesiculation,[16,31−37] and observing supramolecular structures and transformation.[38−42] In a study by Ianiro et al.,[32] a new mechanism for copolymer vesicles was reported during LP-TEM, at which vesicles evolve from spherical micelles formed by polymer-rich liquid droplets (acting as precursors). In a recent study by Touve et al.,[26] the formation and evolution of spherical micelles by the polymerization-induced self-assembly of a diblock copolymer was reported. The electron beam of TEM was used to generate radicals from a polymerizable initiator or iniferter to initiate the monomer polymerization while imaging the formation of structures in the solution. Because of imaging through two 30 nm thick Si_xN_y membranes and thick layer of solvent, the spatial resolution was poor, caused by significant electron beam scattering.

The emergence of graphene liquid cell transmission electron microscopy (GLC-TEM), with the ability to attain the lowest possible solvent thickness and mitigation of the electron radiation-induced damage by graphene layers, significantly improved LC-TEM to attain high-resolution images with minimal sample damage.[43] In this approach, a very thin liquid is trapped between graphene sheets that are impermeable to small molecules, are flexible, and possess excellent thermal and electrical conductivity. Thus, it allows to enhance the signal-to-noise ratio and image resolution, mitigate solvent evaporation under the high vacuum environment of TEM, and minimize sample damage (e.g., charging, degradation, and ionization induced by electron beam radiation).[44,45] Considering the high resolution enabled by a thin liquid layer, Nagamanasa et al.[18] and Bae et al.[25] were able to visualize nanoscale individual polymers in aqueous or organic solution by GLC-TEM.

Herein, we observed the nucleation and evolution of polymer self-assemblies based on a model block copolymer—poly(glycerol methacrylate)-*b*-poly(hydroxypropyl methacrylate) (PolyGMA-*b*-PolyHPMA)—in real time by in-situ GLC-TEM. The PolyGMA−thiocarbonylthio macro-chain-transfer agent (macroCTA) is synthesized by reversible addition−fragmentation chain-transfer (RAFT) method. We speculate that the electron beam of TEM can generate radicals by homolytic cleavage of the thiocarbonylthio group of PolyGMA−thiocarbonylthio macroCTA, which is also reported elsewhere.[26] This causes the initiation of the HPMA polymerization and subsequent self-assembly of the resulting block copolymer within the electron beam irradiated region. Moreover, in view of the full solubility of the PolyGMA homopolymer and HPMA monomer in aqueous solution and under the initial reaction conditions, no organic cosolvent is needed. An unusual property of HPMA is that it is a water-miscible monomer up to 13% w/w at 25 °C, while the corresponding PolyHPMA is insoluble in water.[26] Initially, the growing PolyGMA-*b*-PolyHPMA block copolymer is water-soluble because the PolyHPMA block is relatively short. The hydrophobic character of the PolyGMA-*b*-PolyHPMA block copolymer increases as PolyHPMA becomes longer, leading to induced phase separation and formation of PolyGMA-*b*-PolyHPMA self-assemblies and, ultimately, PolyGMA-*b*-PolyHPMA colloidally stable (sterically stabilized) assemblies.

2. EXPERIMENTAL SECTION

2.1. Raw Materials. Glycerol methacrylate (GMA, 160.2 Da, Polysciences) and hydroxypropyl methacrylate (HPMA, 144.17 Da, 97%, Sigma-Aldrich) were purified before the experiments by passing the liquid through a column filled with basic alumina. All other chemicals including 4,4′-azobis(4-cyanopentanoic acid) (ACVA or V-501, 280.28 Da, ≥98%, Sigma-Aldrich), CD_3Cl (Sigma-Aldrich) containing 1% tetramethylsilane (TMS), deuterium oxide (D_2O, 99.9 atom % D, Sigma-Aldrich), 4-cyano-4-[(dodecylsulfanylthiocarbonyl)sulfanyl]pentanoic acid (CDPA, 403.7 Da, Fisher Scientific), anhydrous ethanol (EtOH, anhydrous, ≥99.5%, Sigma-Aldrich), methanol (Sigma-Aldrich), ultrapure water for chromatography (MilliporeSigma), and diethyl ether (Fisher) are used as received. A UV-lamp (Black-Ray) with a light wavelength and intensity of 360 nm and 100 mW/cm^2, respectively, was used for light-induced copolymerization.

2.2. Synthesis of PolyGMA−Thiocarbonylthio MacroCTA by Reversible Addition−Fragmentation Chain-Transfer (RAFT) Polymerization. The PolyGMA−thiocarbonylthio iniferter or macroCTA was synthesized by RAFT controlled/living radical polymerization of GMA in the presence of CDPA as a RAFT agent. A general mechanism of RAFT controlled/living polymerization is presented in Figure S1. GMA (1 g, 6.2 mmol) and ethanol (2 mL) were added to a 10 mL dry reaction tube containing a stirring rod and CDPA (30 mg, 0.075 mmol) as well as ACVA (2.1 mg, 0.0075 mmol). After purging the solution chilling in an ice bath with argon for around 20−30 min, the reaction tube was transferred to an oil bath preheated at 60 °C. Samples (ca. 0.2 mL) were periodically withdrawn with an argon-purged syringe to monitor the monomer conversion by nuclear magnetic resonance (NMR). After reaching the around target degree of polymerization (D_p) of ∼50 (∼60% monomer conversion), the polymerization was stopped by opening the cap and exposing the polymer solution to air. The synthesized PolyGMA macroCTA was isolated by precipitating in ether as a nonsolvent. The isolated copolymers were redissolved in methanol and reprecipitated in ether. This process was repeated at least three times to ensure that all the impurities (solvent, monomer, and initiator) were removed. The obtained yellow color PolyGMA macroCTA was dried in a vacuum at room temperature.

2.3. RAFT Aqueous Polymerization of HPMA with PolyGMA MacroCTA under UV Light. PolyGMA-*b*-PolyHPMA block copolymer with target D_p ∼ 300 of HPMA ($PolyGMA_{50}$-*b*-$PolyHPMA_{300}$) was synthesized as follows: The as-synthesized PolyGMA macroCTA (0.15 g, 0.019 mmol) from the previous step and HPMA monomer (0.799 mL, 0.82 g, 5.7 mmol) were dissolved in water (10% w/v). The intended D_p of HPMA was 300 (this means that the target polyHPMA has 300 HPMA units). After purging the solution chilling in an ice bath with argon for around 20−30 min, the reaction tube was sealed and exposed to the UV light illumination. 0.2

https://doi.org/10.1021/acs.macromol.2c02318
Macromolecules 2023, 56, 3171−3182

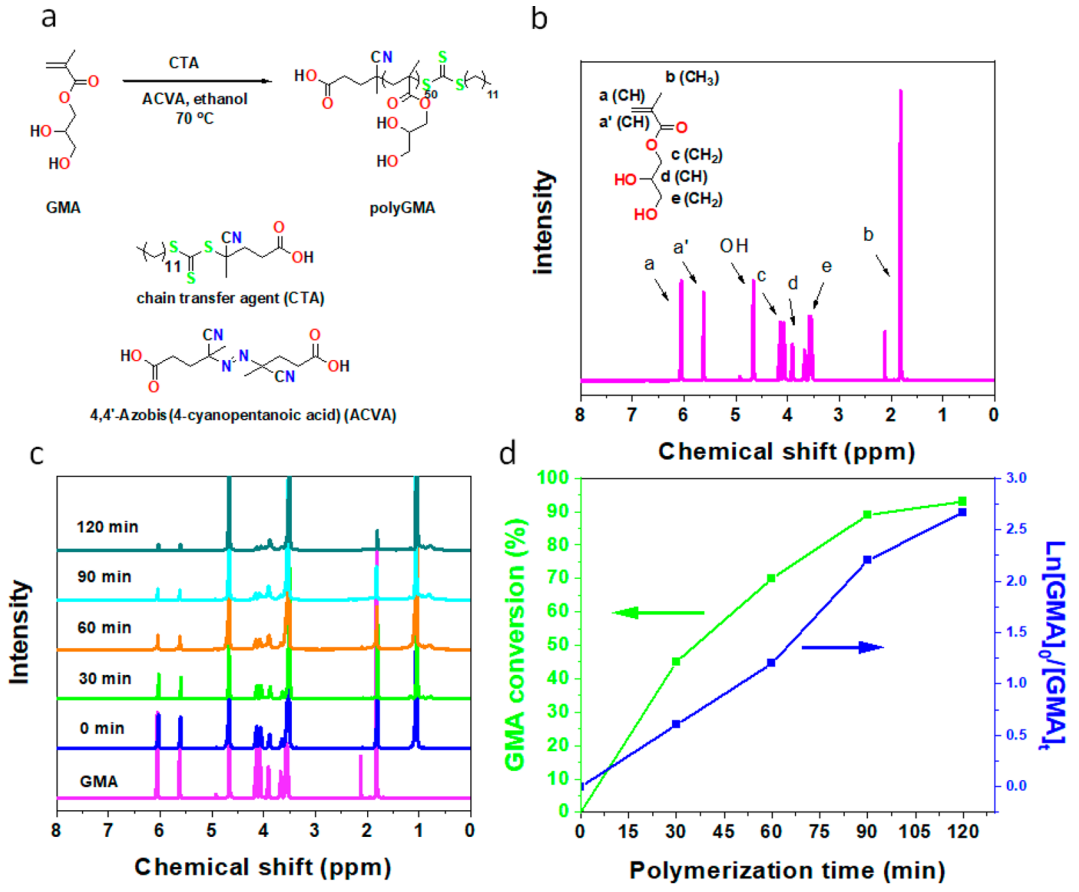

Figure 1. (a) Synthetic procedure for the RAFT homopolymerization of GMA. (b) ^{1}H NMR spectrum of pure GMA monomer. (c) Time-dependent RAFT polymerization of GMA analyzed by ^{1}H NMR. (d) Kinetics of the GMA homopolymerization: GMA conversion vs time and the semilogarithmic plots for the PolyGMA homopolymer synthesis using $[GMA]_0$ = 40% w/v, target D_P = 80, and actual D_P = 50 (at ∼60% conversion) in ethanol at 60 °C using the RAFT agent and ACVA initiator (CTA/ACVA molar ratio is 5:1). $[GMA]_0$ and $[GMA]_t$ represent the initial GMA monomer concentration and after time t, respectively. The linearity in the semilogarithmic plot shows first-order kinetics.

mL aliquots were taken from the solution and diluted around 10 times in water for the dynamic light scattering (DLS) measurements. Particle growth kinetics analysis was performed using a Malvern Zetasizer Nano ZSP.

2.4. Dry-State Transmission Electron Microscopy (TEM). A small aliquot (1 μL) of the sample was manually pipetted onto a TEM grid (carbon-coated 300 copper mesh, Sigma-Aldrich). Excess solution was removed by blotting the edge of the grid with filter paper, and then the sample-loaded grid was dried by evaporation at room temperature. The TEM imaging was performed on a JEM-ARM200 (JEOL, Ltd.) operated at 200 keV, and micrographs were recorded on 2K × 2K Orius SC200 CCD camera (Gatan Inc.).

2.5. Protocol for Preparation of Graphene-Coated TEM Grids. A detailed explanation for the preparation of graphene-coated TEM grids and their characterization was reported in our previous work.[46] A general protocol was as follows: 200 or 300 mesh carbon-coated Au grids from carbon-coated side were gently placed onto a small piece of a smooth graphene-on-Cu foil. Having a smooth surface ensures a good contact between the graphene layer and carbon layer of the Au grid. Then, a few drops of isopropanol were poured onto the grids or foil and allowed to dry for approximately 2−3 h. Isopropanol ensures a good contact between the carbon film on the Au grids and the coating graphene layer. Then, the Cu foil was etched by gently laying down a graphene-on-Cu piece on the $Na_2S_2O_8$ etching solution (made of 1 g of $Na_2S_2O_8$ in 10 mL of ultrapure water) and kept for approximately 20 h. In the last step, the floating graphene-coated Au grids were removed and rinsed with water (in a Petri dish) at least three times to ensure full removal of the etched Cu. Afterward, the graphene-coated Au grids were dried under a lamp or at ambient temperature.

2.6. Protocol for Making Liquid Cell Pockets for GLC-TEM Experiments. GLC was formed by putting a small droplet (∼0.2 μL) of the polymer aqueous solution onto a graphene-coated TEM grid, and the second graphene-coated TEM grid was gently located on top of the bottom grid. Excess solution was removed by blotting the edge of the grid with filter paper, followed by laying a top graphene chip, or cover chip, onto the bottom chip, leading to producing the creases in the top graphene sheet and trapping the liquid. The graphene sheets provide the required mechanical integrity for the liquid pockets.[46]

2.7. Visualization of PolyGMA-*b*-PolyHPMA PISA by GLC-TEM. The as-synthesized PolyGMA macroCTA from the previous step was used for the polymerization-induced self-assembly of PolyGMA-*b*-PolyHPMA copolymers. PolyGMA macroCTA (0.15 g, 0.019 mmol) and HPMA (0.799 mL, 0.82 g, 5.7 mmol) were dissolved in deionized water (10% w/v). The resulting solution while chilling in an ice bath was purged with argon for around 20−30 min. The liquid pockets were made by pipetting out a small aliquot (0.2−0.3 μL) of the solution onto a graphene chip (graphene-coated copper, Graphenea Inc.). Excess solution was removed by blotting the edge of the grid with filter paper, followed by laying a top graphene chip, or cover chip, onto the bottom chip, leading to producing the creases in the top graphene sheet and trapping the liquid. The TEM grid that graphene sheets were coated onto provided the required mechanical integrity. The GLC-TEM imaging was performed on a JEM-ARM200 (JEOL, Ltd.) operated at 200 keV, and micrographs were recorded on a 2K × 2K Orius SC200 CCD camera (Gatan Inc.). The electron beam radiation induced HPMA polymerization within

https://doi.org/10.1021/acs.macromol.2c02318
Macromolecules 2023, 56, 3171−3182

the liquid pockets where nucleation and evolution of PolyGMA-*b*-PolyHPMA self-assemblies were directly imaged. The same concentration of the polymer solution was pipetted onto the carbon-coated TEM grid and the graphene-coated TEM grid for the ex-situ and in-situ micelle formation experiments, respectively.

2.8. ^{1}H NMR Spectroscopy. ^{1}H NMR analyses were performed on a Bruker Avance 500 NMR spectrometer. GMA and the PolyGMA samples were prepared in D_2O solvent; HPMA and PolyGMA-*b*-PolyHPMA copolymerization samples were prepared in $(CD_3)_2SO$ solvent. ^{1}H NMR spectrum of the CDPA CTA (Figure S2) indicates signals at chemical shifts of 3.4, 2.7, 2.4−2.6, 1.9, 1.7, 1.2−1.50, and 0.9 ppm.[47]

3. RESULTS AND DISCUSSION

3.1. Synthesis of PolyGMA−Thiocarbonylthio Macro-CTA by RAFT Polymerization. Generally, two major strategies have been investigated for preparation of polymeric nanomaterials: self-assembly of polymers in a selective liquid medium and heterogeneous polymerization such as emulsion and dispersion polymerization.[48,49] Unlike the first approach which requires multistep synthesis and troublesome purification and is also limited to a very dilute solution (e.g., 1% w/v solid content), heterogeneous polymerization is a single-step facile approach that facilitates the visualization of nucleation and evolution of polymeric self-assembled structures during polymerization. Dispersion polymerization-induced self-assembly (PISA) is a simple and scalable method for synthesizing nanoscale soft, organic materials with various morphologies and size at high polymer concentrations, up to 50% w/v.[14,48,49] In this method, the hydrophilic block of a multiblock copolymer is synthesized by a controlled/living polymerization technique (e.g., RAFT), followed by addition of the hydrophilic monomer that polymerize into the hydrophobic block. At the early stage, the homogeneous polymerization results in the formation of the hydrophobic block polymer. Later on and due to hydrophobicity of the growing polymer chain and increasing length ratio of hydrophobic to hydrophilic blocks, phase separation takes place and polymer chains aggregate (homogeneous polymerization transit into a dispersion polymerization), and the resulting block copolymer self-assembles into nanoscale structures. As a result of constant polymer chain growth, a series of morphologies are expected to be observed during self-assembly trajectory with the spherical micelles being the first typical morphology.

In this study, preparation of PolyGMA-*b*-PolyHPMA amphiphilic copolymers with PolyGMA as water-soluble block and PolyHPMA as water-insoluble block is performed in two steps: First, PolyGMA−thiocarbonylthio iniferter or macroCTA is synthesized by controlled/living RAFT polymerization of GMA, and then the synthesized PolyGMA macroCTA is used for controlled/living RAFT polymerization of HPMA monomer in aqueous solution. PolyGMA−thiocarbonylthio macroCTA homopolymerization is performed under heat, and the RAFT polymerization of PolyHPMA is performed under UV light irradiation (ex situ) or electron beam irradiation (in situ). RAFT polymerization is chosen because it allows a facile radical polymerization under electron beam radiation during the direct TEM imaging. A schematic illustration of the reaction conditions for RAFT homopolymerization of PolyGMA macroCTA with a target block degree of polymerization (D_P) of 83 and actual $D_P \sim 50$ (at ∼60% conversion) is shown in Figure 1a. The ^{1}H NMR spectra of pure GMA monomer and the PolyGMA−thiocarbonylthio macroCTA at different polymerization times are also given in Figures 1b and 1c. All the signals associated with the GMA and PolyGMA macroCTA in the RAFT polymerization medium are observed in each of the sample's spectrum: 6.10 ppm (1H, CH), 5.60 ppm (1H, CH), 4.1 ppm (2H, $-CH(OH)-CH_2-O-$), 3.9 ppm (H, $-CH(OH)-$), 3.5 ppm (2H, $-CH(OH)-CH_2-O-$), 1.8 ppm (3H, $CH_3-C=CH_2$) ppm. All other signals (around 1.1, 3.6, and 4.7 ppm) are related to either ethanol solvent or residual D_2O solvent. The appearance of new broad signals at around 0.8−1 and 3.8−4.2 ppm can be correlated to the PolyGMA. The ^{1}H NMR spectrum of PolyGMA powder (Figure S3) synthesized by precipitation in ether shows signals at around 3.7 ppm (2H, $-O-CH_2-$), 3.9 ppm (1H, $-CH_2-CH(OH)-$), 3.4 ppm (2H, $CH_2(OH)-CH(OH)-$), 1.8 ppm (2H, $-CH_2-C(CH_3)-$), and 0.8−1 ppm ($CH_3-C(CH_2)-$).[50,51] The signals at around 4.7 and 4.9 ppm are correlated to the OH groups. The signal at chemical shift of ∼2.5 ppm can be attributed to the residual d-DMSO solvent.

The conversion rate of the GMA monomer is calculated by integrating the area under peak of the vinyl CH signals (5.6 or 6.10 ppm) versus the PolyGMA peaks (Figures 1c,d and S3) or versus CDPA (Figure S4). It is important to note that all the signals of the CDPA overlap with the GMA or PolyGMA signals, except the region around 2.2−2.6 ppm (related to four protons of the CDPA) which is used for the GMA monomer conversion calculations. Before the polymerization, the molar ratio of GMA is around 83 times compared to CDPA. This means that there should around 83:4 or around 20 times more vinyl protons of GMA compared to the four protons of CDPA (shown in 2.2−2.6 ppm). The GMA:CDPA molar ratios after 30, 60, 90, and 120 min of polymerization times are around 44, 68, 89, and 95%, respectively. This indicates that the calculated GMA conversion rates using end groups (CDPA) are consistent with the GMA conversion rate calculated by integrating the area under the peak for vinyl protons and the forming PolyGMA (shown in Figure 1d) and intended D_p. The increased ratio of the CDPA signal compared to the vinyl signals being consumed during polymerization further indicates continuous GMA polymerization. According to the kinetics of GMA homopolymerization (GMA conversion rate versus polymerization time in the semilogarithmic plot) shown in Figure 1d, the linearity in the semilogarithmic plot shows first-order kinetics (linear increase in the conversion rate with respect to the polymerization time).[52,53] This means that the PolyGMA polymerization complies with controlled/living polymerization criteria (linear increase in the semilogarithmic conversion rate with respect to the polymerization time). Moreover, as often found for RAFT polymerization synthesis,[15,52,54−56] a short induction period is observed for the RAFT polymerization of GMA. Controlled/livingness of the RAFT dispersion polymerization of HPMA is key to the phase separation, self-assembly, and morphological transitions in a PISA process.

3.2. UV-Light-Triggered Synthesis of PolyGMA-*b*-PolyHPMA Block Copolymer. To assess the morphological features of electron beam radiation-induced PolyGMA-*b*-PolyHPMA self-assemblies during in-situ GLC, the copolymer is synthesized ex-situ under UV-light irradiation. UV-light-induced and electron-beam-induced RAFT copolymerizations of PolyGMA and HPMA are schematically shown in Figure S6. A similar concentration of the polymer solution used for the light-induced RAFT copolymerization is drop-casted onto the dry-state TEM grid and the GLC-TEM grid for the ex-situ and

https://doi.org/10.1021/acs.macromol.2c02318
Macromolecules 2023, 56, 3171−3182

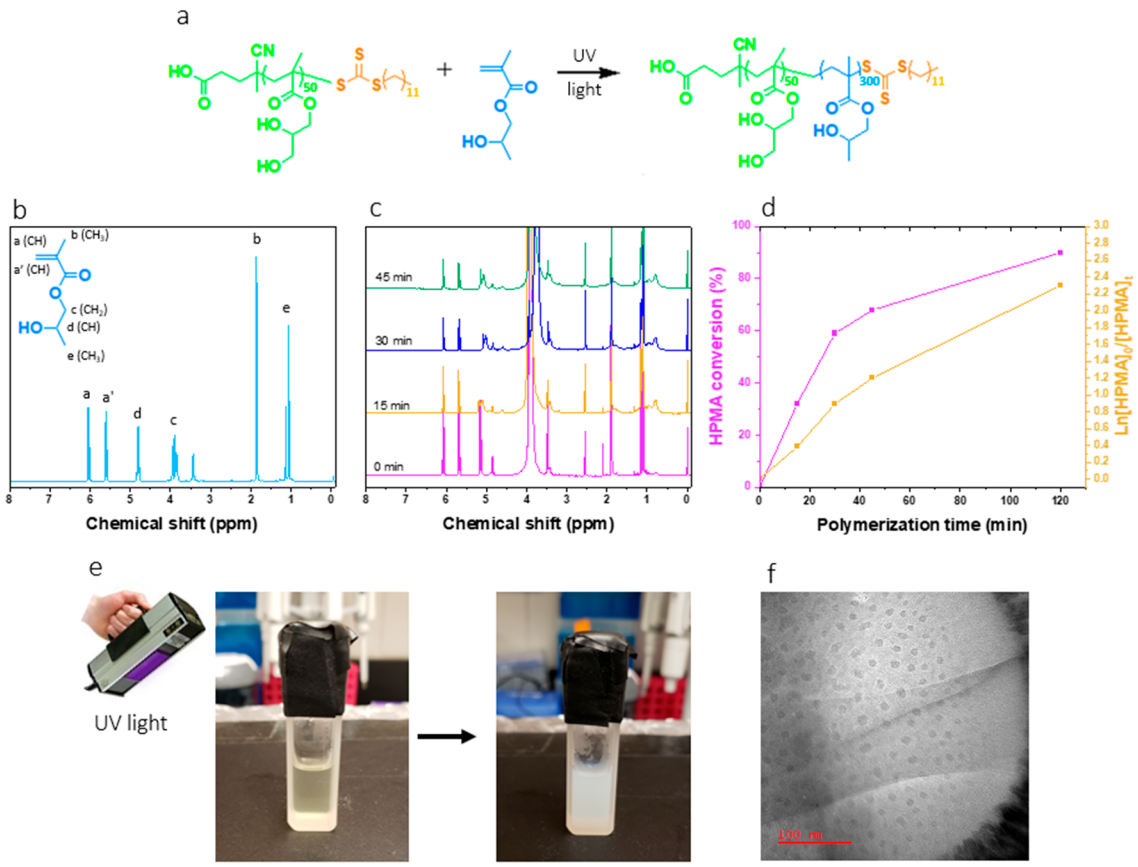

Figure 2. Preparation of PolyGMA-*b*-PolyHPMA copolymer under UV light irradiation and morphological study of the self-assembled structures. (a) Schematic illustration of UV-light-induced polymerization of HPMA in the presence of PolyGMA macroCTA. (b) ^{1}H NMR spectrum of pure HPMA monomer. (c) Time-dependent RAFT copolymerization of HPMA analyzed by ^{1}H NMR. (d) Kinetics of the HPMA copolymerization. HPMA conversion vs time and the semilogarithmic plots for the PolyHPMA ($[HPMA]_0$ = 10% w/v; target D_P = 300; in water using the RAFT agent (HPMA/PolyGMA molar ratio is 300). $[HPMA]_0$ and $[HPMA]_t$ represent the initial HPMA monomer concentration and after time *t*, respectively. The linearity in the semilogarithmic plot shows first-order kinetics. (e) Photo image of the copolymerization medium (PolyGMA and HPMA in water) before and after copolymerization. (f) Dry-state TEM image of PolyGMA-*b*-PolyHPMA copolymer micelles formed under UV-light irradiation.

in-situ polymer self-assembly experiments, respectively. A schematic illustration of the RAFT polymerization of HPMA in the presence of PolyGMA macroCTA is shown in Figure 2a. The ^{1}H NMR spectrum of pure HPMA monomer is given in Figure 2b. The signals are observed at 6.10 ppm (1H, vinyl), 5.60 ppm (1H, vinyl), 4.8 ppm (1H, $-CH(OH)-CH_3$), 3.9 ppm (2H, $-CH_2-CH(OH)-$), 1.9 ppm (3H, $CH_3-CH(OH)$), and 1.2 ppm (3H, $CH_3-C=CH_2$). The signal at the chemical shift of ~2.5 ppm can be attributed to the residual d-DMSO solvent. The ^{1}H NMR spectrum of the copolymerization medium composed of pure HPMA monomer and the PolyGMA−thiocarbonylthio macroCTA in water (10% w/v) at different polymerization times is also given in Figure 2c. The weak signals of the PolyGMA are overlapped by the signals related to the HPMA or water solvent, except a weak signal at chemical shift of around 0.8−1 ppm ($CH_3-C(CH_2)-$) which can be easily distinguished. The conversion rate of the HPMA monomer (Figure 2d) is calculated by integrating the area under peak of the vinyl CH signals (5.6 or 6.10 ppm) versus the PolyHPMA peaks (around 4.6−4.8 ppm) or versus PolyGMA macroCTA. It is also important to note that the ratio of the PolyGMA signal versus the vinyl signals increases as the copolymerization proceeds, further indicating the constant copolymerization. Furthermore, the chemical shift of the water proton peak is typically observed ~4.7 ppm, and herein the proton peak is slightly upfield shifted caused by paramagnetic shift effects.[57,58]

It should be noted that prior to the copolymerization, the aqueous solution containing PolyGMA macroCTA and HPMA is homogeneous and clear (Figure 2e). During initial stage of copolymerization, the growing PolyGMA-*b*-PolyHPMA copolymer with short PolyHPMA block is also water-soluble. It is important to note that the chain length of the PolyGMA macroCTA is fixed throughout the copolymerization. When the chain length of PolyHPMA block reaches a critical value[26] (instability of free polymers in solution influenced by the chain length), microphase separation occurs to induce molecular self-assembly and the formation of polymer nanostructures. Thus, the mixture turns translucent and opaque, and with further progress of the HPMA polymerization, the polymerization mixture becomes white. This observation can also denote the increase in number as well as size of the self-assembled polymer nanomaterials. The dry-state TEM micrographs of PolyGMA-*b*-PolyHPMA self-assembled micelles with no staining (Figure 2f) indicate the assembly of the block copolymer into spherical micelles. According to the image analysis results (Figure S7), the polymer assemblies have an average size of 14 nm. This micellar particle size is similar to

https://doi.org/10.1021/acs.macromol.2c02318
Macromolecules 2023, 56, 3171−3182

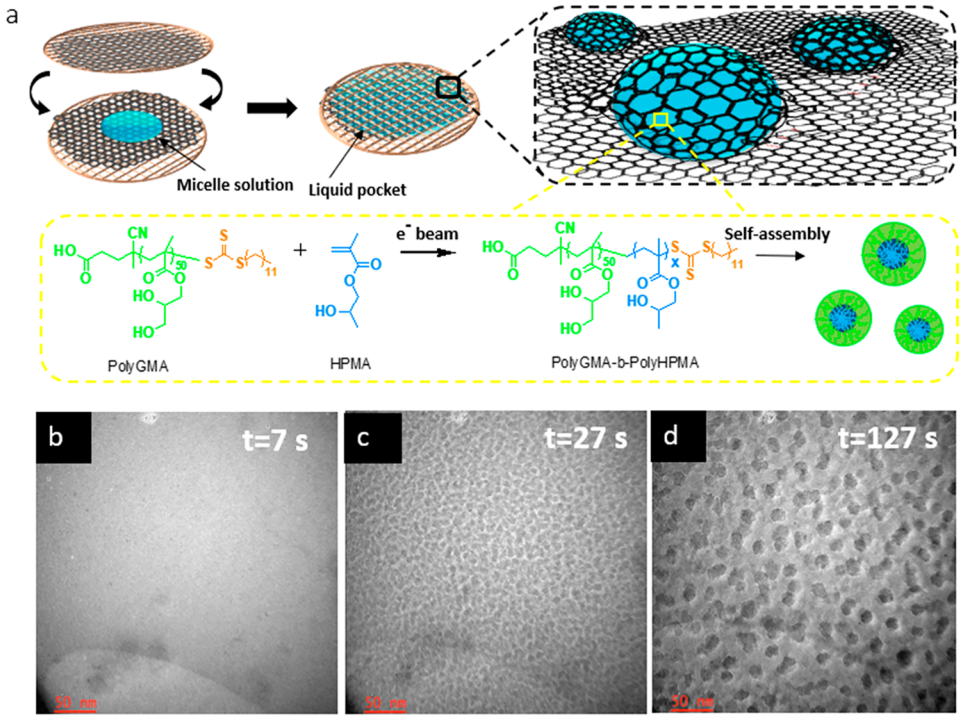

Figure 3. Nucleation and evolution of PolyGMA-*b*-PolyHMPA block copolymer micelles acquired by in-situ GLC-TEM. (a) Schematic illustration of the formation of liquid pockets (aquaous solution of polyGMA and HPMA) between graphene layers of the graphene-coated TEM grids. (b–d) Time-lapse sequential TEM images taken during an in-situ GLC-TEM experiment of an aqueous solution of HPMA and PolyGMA macroCTA forming PolyGMA-*b*-PolyHMPA block copolymer micelles obtained from Movie S2. The solution is continuously irradiated by the electron beam.

the block copolymer micelles formed under UV-light reported elsewhere.[59] It should be also noted that the imaged assemblies are in the dry state (after drying solvent), at which the final sizes could be influenced by rearrangement of polymer chains (especially PolyGMA hydrophilic corona) to form denser structures as result of solvent removal. Furthermore, we have measured size of the polymer assemblies by DLS as shown in Figure S8. According to the DLS results, the hydrated micelles have an average size of 42, 51, 57, and 102 nm after 15, 30, 45, and 120 min of UV light irradiation. Similar sizes of the hydrated assemblies measured by DLS are reported by Touve et al.[26] for micelles formed from copolymerization of poly(ethylene glycol) macroCTA and HPMA under UV light.

3.3. In-Situ Observation of Molecular Self-Assemblies during GLC-TEM Imaging. Our speculation is that PISA of the PolyGMA-*b*-PolyHPMA block copolymer is also triggered by the electron beam radiation during GLC-TEM imaging, allowing simultaneous formation and visualization of molecular self-assemblies, as also reported elsewhere.[26] In contrast to the ex-situ-prepared PolyGMA-*b*-PolyHPMA micelles, this approach allows direct visualization of the polymer particles as they are assembling from the growing copolymer amphiphiles in solution. Beside the imaging mode, GLC-TEM videography is also performed to visualize the nucleation and evolution of the polymer self-assemblies. Figure 3a schematicly illustrates the formation of liquid pockets (aquaous solution of polyGMA and HPMA) between graphene layers of the graphene-coated TEM grids. For the first step, we examined the possibility of the PolyGMA-*b*-PolyHPMA micelles formation under TEM. Thus, we image the control solutions by removing one component from the polymerization solution. Each control solution is imaged at the same imaging conditions as PolyGMA-*b*-PolyHPMA solution. One of the control experiments included a solution containing only PolyGMA–trithiocarbonate macroCTA (no HPMA) in water to ensure no particle formation observation (Figure S9). As can be seen, no structure or noticeable change in the solution is observed. The presence of water in a liquid cell can be verified by electron energy loss spectroscopy (EELS)[46,60–62] to measure water exciton or oxygen, bubble formation,[60,61] and liquid thickness measurement.[60,61] The presence of water in GLC during the TEM imaging of the PolyGMA aqueous solution is confirmed by EELS as shown in Figure S10. Low loss EELS data exhibit a peak ∼7 eV related to the water optical gap, a peak ∼9 eV related to water exciton, a peak ∼14 eV related to graphene $\sigma+\pi$ bond, and a peak ∼24 eV for the plasma maxima of water.[46,60–62] The presence of bubbles (Movie S1) further indicates the presence of water in the GLC. Indeed, bubbles have very distinct contrast (white or colorless) compared to the surrounding liquid area (dark contrast). In the other control experiment, an aqueous solution containing only HPMA (no PolyGMA–trithiocarbonate macroCTA) is tested (Figure S11). Similar to the previous case, no structure or noticeable change in the solution is observed. Similar observations (no assembly formation) are reported by Touve et al.[26] for the control experiments of pure HPMA in water as well as pure poly(ethylene glycol) macroCTA in water. According to our observations, we infer that the formation of self-assembled structures requires the presence of an easily dissociable molecules (such as iniferter or macroCTA) and a monomer to polymerize.

In the next step, we investigate the formation of PolyGMA-*b*-PolyHPMA micelles under electron beam of TEM while imaging the copolymer solution. Under continuous imaging conditions at an electron dose of ∼1.2 $e^-/(Å^2\ s)$, the micellar particles are observed to form in the small pockets of GLC and

https://doi.org/10.1021/acs.macromol.2c02318
Macromolecules 2023, 56, 3171–3182

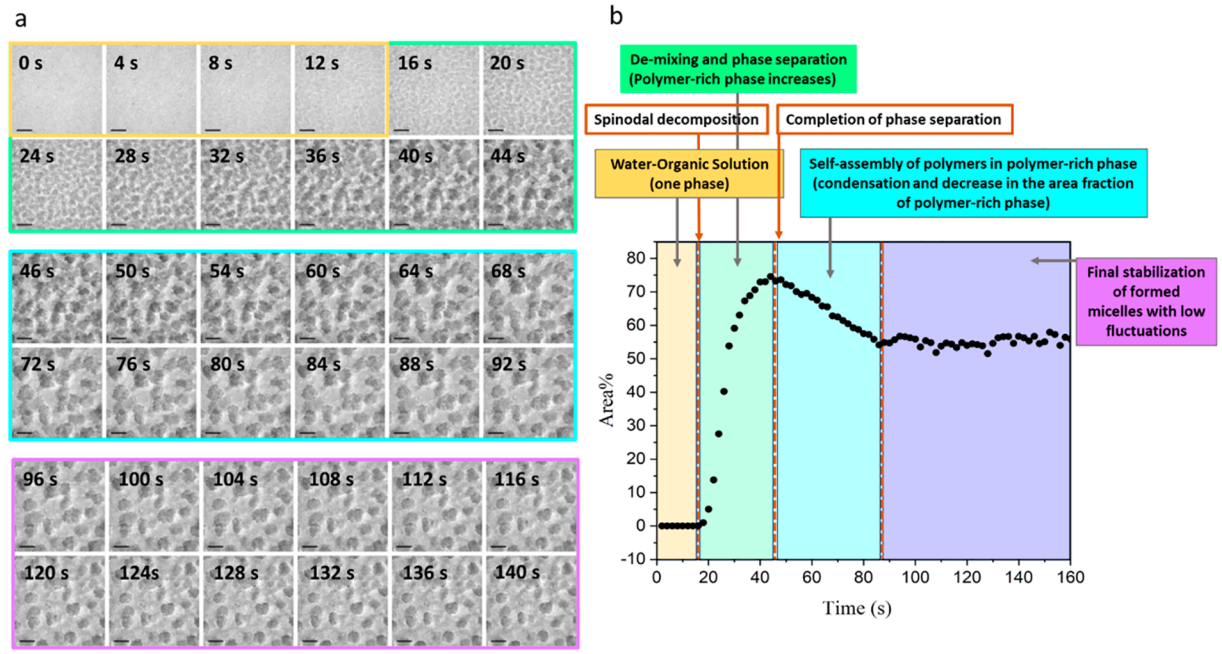

Figure 4. Spinodal decomposition mechanism proposed for the formation of PolyGMA-*b*-PolyHPMA micelles. (a) Time lapse sequential TEM images taken during an in-situ GLC-TEM experiment for the formation of PolyGMA-*b*-PolyHMPA copolymer micelles from an aqueous solution of HPMA and PolyGMA macroCTA. TEM images are taken from Movie S2. Scale bar is 20 nm. (b) Corresponding area plot for the evolution of the PolyGMA-*b*-PolyHMPA micelles.

grew over time. The change in image contrast can be attributed to the rearrangement of the copolymers aggregates into micelles with a dark contrast core surrounded by a lighter contrast solvated corona. During the initial stage, PolyGMA–thiocarbonylthio macroCTA and HPMA are both water-soluble, and the solution appears free of any polymer assembly (Figure 3b). It is important to note that an unusual property of HPMA is that it is a water-miscible monomer up to 13% w/w at 25 °C, while the PolyHPMA is water-insoluble.[26] At initial stages of the molecular self-assemblies, the growing PolyGMA-*b*-PolyHPMA block copolymer is water-soluble because PolyHPMA block is relatively short (Figure 3b). The block hydrophobic character increases as the propagating chains become longer, leading to induced microphase separation and the formation of faint polymer aggregates or structures (Figure 3c). In a recent work, it is also reported that the polymer aggregates look darker in contrast to the background (surrounding liquid medium).[18] Ultimately, PolyGMA-*b*-PolyHPMA transit into colloidally stable (sterically stabilized) micelles (Figure 3d). The last step minimizes the surface tension at the water–PolyHPMA interface. The shape and size of the PolyGMA-*b*-PolyHPMA micelles formed in GLC (Figure 3d) are similar to the micelles formed under standard conditions (Figure 2f). The formation of nanoscale micelles with a rough spherical morphology synthesized experimentally by LC-TEM and calculated theoretically by molecular dynamics (MD) simulation is also reported in the previous works.[26,55,63]

To have a controlled polymerization chemistry, it is critical to ensure that the concentration of radicals formed via cleavage of thiocarbonylthio molecules is significantly greater than that of radicals formed from the water radiolysis induced by the electron beam. The electron dose used in this study is up to ~1.2 $e^-/(Å^2\ s)$, which is equivalent to ~48 × 10^5 Gy/s at 200 keV acceleration voltage. Water radiolysis can lead to the formation of radical species and other types of molecular species such as H_3O^+, OH^-, e^-_{aq}, $OH^•$, $H^•$, H_2O_2, H_2, and HO_2.[59,64] Roughly estimated steady-state concentrations of predominant radiolysis species (H_2O_2, H_2) at this electron dose can be less than 7 × 10^{-5} M in the beam-irradiated region within the liquid cell at 300 eV acceleration voltage.[59,64,65] This value is expected to be much lower at 200 eV acceleration voltage, which is used in this study. Moreover, the steady-state concentrations of radical species (e.g., $OH^•$ and $H^•$) could be estimated at orders of magnitude lower than the predominant radiolysis species. The concentration of the PolyGMA–thiocarbonylthio molecules in the aqueous solution during GLC-TEM experiment is ~2.4 × 10^{-3} M. Therefore, if we assume that all the PolyGMA– thiocarbonylthio molecules within the beam-irradiated region cleave rapidly with equal likelihood of beam-induced cleavage, then the concentration of PolyGMA–thiocarbonylthio molecule-derived radicals would be significantly higher than concentration of the solvent radiolysis product. Hence, we speculate that the radical polymerization primarily results from the cleavage of thiocarbonylthio molecules.

We have also studied the electron dose effect on the polymer assemblies. Movie S2 is collected with an approximate electron dose of ~1.2 $e/(Å^2\ s)$, and Movie S3 is collected with a lower electron dose of ~0.8 $e/(Å^2\ s)$. As can be seen from Movie S3, a similar size and shape for assemblies are observed when compared to the higher electron dose. However, the polymer assemblies form at a slower rate under lower electron dose which could be correlated to the slowed radicals formation through cleavage of PolyGMA–thiocarbonylthio molecules and, hence, a slowed HPMA radical copolymerization. We also speculate that the electron beam can affect livingness of polymer chains, and D_p of PolyHPMA might not reach 300 (target value), which can account for observation of micelles with smaller diameters, especially when compared to the

https://doi.org/10.1021/acs.macromol.2c02318
Macromolecules 2023, 56, 3171–3182

micelles formed under standard condition measured by DLS. Yet, because the micelles formed under different imaging conditions show almost the same size and shape, it can be speculated that the smaller diameter of micelles may be due to limited micelles aggregation numbers rather than the formation of polymers with lower D_p. A similar behavior is reported by Touve et al.[26] for micelles formed from copolymerization of poly(ethylene glycol) macroCTA and HPMA, whereas sizes of hydrated micelles measured by DLS were greater than the sizes of micelles observed under the electron beam.

In general, continuous growth of the self-assemblies can be as a result of a single or combination of pathways such as monomer addition[22,66,67] or micelle−micelle coalescence/fusion.[68−71] Considering the very rapid reaction kinetics, it is very hard to distinguish individual particles during initial copolymerization stages. We believe that the mechanism of the micellar evolution could be explained via spinodal decomposition (defined as spontaneous separation of a single thermodynamic phase into two phases as result of very small thermodynamic barrier for the phase separation). Figure 4 shows analysis of the polymer assemblies evolution based on spinodal decomposition mechanism. According to the TEM snapshots shown in Figure 4a, the copolymerization medium is initially a homogeneous single phase (up to 16 s). It should be noted that during the initial stage, PolyGMA macroCTA and HPMA are both water-soluble, and the growing PolyGMA-*b*-PolyHPMA copolymer with short PolyHPMA block is also water-soluble. Afterward, the phase separation by spinodal decomposition starts and converts the mixture into two phases of a polymer-rich and a water-rich (polymer-poor) phase. The polymer-rich phase appears darker, and the water-rich phase appears brighter. In fact, the block hydrophobic character increases as the propagating PolyHPMA chains become longer, inducing microphase separation and the formation of faint polymer aggregates or assemblies.[26] Observation of small aggregates at the initial stage of the micelle formation (Figure 4a) could result from the PolyGMA-*b*-PolyHPMA copolymer with a relatively short PolyHPMA block. With further progress of the HPMA polymerization, the polymer assemblies form mature, round-shaped micelle structures to minimize the surface tension between hydrophobic PolyHPMA block and water molecules. This could be also indicated by the copolymerization mixture becoming white at later copolymerization stages (Figure 2e).

To further investigate mechanism of the polymer self-assemblies, we have measured and plotted the area fraction of polymer-rich region (darker region) over time as shown in Figure 4b. The phase separation happens by appearance of the darker region (around t = 16 s) and continues by a fast increase in the area fraction of polymer-rich area (until around t = 46 s). After this point, phase separation is completed (from around t = 46 s until t = 86 s), and the area of the polymer-rich region decreases at a constant rate. After formation of stable micelles (around t = 86 s), the area fraction of the polymer-rich region does not change significantly. The TEM snapshots (Figure 4a) show that coalescence between small assemblies is observed toward forming micellar assemblies. Also, it can be seen the darker regions are condensing to form compact, sphere-like 3D assemblies. The single particle tracking (Figure S12) shows that initial micelles are transforming into more compact micelles which we speculate to be correlated to the polymer chains rearrangements to enhance thermodynamic stability. This could explain why ex-situ-synthesized micelles have slightly smaller average size when compared to the in-situ-formed micelles (Figure S7). It can be expected that, upon further aging, the in-situ-formed micelles reach the same size of the ex-situ-formed micelles.

Using a PolyGMA macroCTA with a fixed chain length, a systematic increase in chain length of the PolyHPMA block with respect to the polymerization time leads to an increase in the diameter of micellar particles. In general, continuous growth of the self-assemblies can be as a result of a single or combination of pathways such as unimer addition[22,66,67] or micelle−micelle coalescence/fusion.[68−71] The observed slow growth of some of the micelles can be attributed to a concentration gradient or sluggish movement of the reacting species such as HPMA monomer and the growing PolyGMA chain. It also appears that some of the PolyGMA-*b*-PolyHPMA micelles did not have enough time to rearrange and form a dense core. Polymer micelles with no distinct core and corona are also reported in the previous studies.[17,19,26,63] Indeed, electron microscopy imaging of bare polymer structures is rather challenging due to their small size, low image contrast, and propensity for chemical decomposition under focused electron beam radiation.[17−19,26,63] The aged, dried copolymerization sample prepared under UV light (Figure S13) clearly indicates the formation of large micelles with a distinct core and corona. Similar polymer assemblies with irregular shapes, sizes, or shell thickness are reported in the previous literature,[17,52,53,56,63,72] which could be correlated to compound micelles formation as result of micellar fusion or transformation into other assembled structures or structural damage induced by electron beam during TEM imaging.

Generally, the formation of block copolymer assemblies is primarily dependent on thermodynamic rule, whereas the change of free energy (ΔG) must be negative.[73] As for the spherical micelles formation, enthalpy change (ΔH) with a negative value is desirable. This is mainly because of a stronger affinity that exists among PolyHPMA blocks than of that between the blocks and solvent. This desirable enthalpy change can also be ascribed to the corona-forming PolyGMA blocks as a result of an increase in polarity of the medium upon the HPMA monomer consumption. In view of the conformational change in both PolyHPMA and PolyGMA blocks, the entropy (ΔS) contribution to the formation of micelles is undesirable. Nevertheless, the change of the solution composition might lead to a negative entropy value. Overall, the formation of PolyGMA-*b*-PolyHPMA micelles in the solution is thermodynamically spontaneous. Similar to the previous report by Eisenberg et al.,[74] the formation of micellar aggregates can be under control of the stretching degree of PolyHPMA core-forming block (entropy concern), the repulsion interaction of PolyGMA corona-forming block (enthalpy and entropy concerns), and interfacial energy of core−corona (enthalpy concern). In this work, the chain length of PolyGMA block is fixed, indicating that the enthalpy contribution from the hydrophilic blocks is unchanged throughout the polymerization. The interfacial energy of core−corona is product of interfacial area and interfacial tension, where the former has the tendency to a minimum value and the latter is constant. Additionally, the PolyHPMA block should further stretch upon increase in the PolyHPMA chain length, especially in the core area next to the interface, leading to protuberance of the core-forming PolyHPMA block into the surrounding medium.[75] Hence, deformation of PolyGMA-*b*-PolyHPMA spherical

https://doi.org/10.1021/acs.macromol.2c02318
Macromolecules 2023, 56, 3171−3182

micelles, aggregation and coalescence, and also transition into other morphologies can be expected.

We have also observed that some of the micelles intermittently disappear prior to reappearing into the solution (Figure S14). This can be due to movement of the micelles within the volume of the electron irradiated region of the GLC or due to a slight change in the hydrophobic core density or transient crystallization of the glassy core during the assembly growth. The micelles growth can be mainly explained by gradual attachment of the copolymer molecules rather than coalescence of the smaller micelles.[63,76] A similar observation is reported by Touve et al.[26] during SiN LC-TEM imaging of polymer micelles within thick SiN membranes. Nagamanasa et al.[18] also have reported detachment of polymer molecules from the surface of GLC window followed by readsorption. Bae et al.[25] introduced a particular functionality as electron-rich pendant groups are also introduced within the polymer chains to enhance image contrast as well as surface (attractive) interactions between the functionalities and graphene layer of the GLC, enabling visualization of molecular rearrangement or movement of single polymer chains. It should be also noted that the graphene layer around the liquid pockets does not significantly affect the micelle growth.[77] Furthermore, no significant bubble formation or sample decomposition is observed during GLC-TEM imaging.[18] Minimizing electron dose during LC-TEM imaging is crucial, especially for soft matter nanostructures, as high dose rates can lead to beam-related artifacts, influencing motion of individual objects, change equilibrium and kinetics across a system, change the solution chemistry via radiolysis, and create other reactive species.[23,65,78,79] Decreased electron dose could result in poor resolution of low-contrast soft/organic matter including polymer self-assemblies.[26] Yet, high electrical and thermal conductivity of graphene layers (compared to Si_xN_y membranes) lead to distribution of the locally irradiated electron beam and minimize the occurrence of the parasitic side reactions.[18,43] This allows imaging under relatively higher electron flux using GLC, leading to high-resolution imaging.

In short, we have shown that organic reactions (molecular structures formed by self-assembly in this case) can be initiated and visualized by GLC-TEM in real time. Because of many advantages of graphene layer (e.g., impermeable to small molecules, flexible, excellent thermal and electrical conductivity), GLC-TEM is demonstrated as a promising approach to study electron beam-sensitive soft/organic matter such as polymers and proteins. More developments in experimental design, liquid cell design, imaging conditions, and data analysis can further facilitate our understanding related to dynamics of organic reactions.

4. CONCLUSIONS

In summary, we demonstrate the formation and visualization of molecular self-assemblies during organic reactions by GLC-TEM in real time. The graphene layer of the liquid cell offers encapsulating an ultrathin liquid layer containing organic reactants, enabling a high-contrast imaging with mitigated electron-beam-induced damage. GLC-TEM is successfully used to induce as well as visualize polymerization-induced self-assemblies of PolyGMA-*b*-PolyHPMA block copolymer in aqueous solution. It is our inference that electron beam radiation homolytically cleaves the PolyGMA−thiocarbonylthio macroCTA initiating living/controlled RAFT polymerization of HPMA. Continuous chain growth of the hydrophobic PolyHPMA block and subsequent microphase separation leads to the formation of nanoscale PolyGMA-*b*-PolyHPMA self-assemblies. We believe that the mechanism of the micellar evolution could be explained via spinodal decomposition, whereas the initial single phase transform into two phases of a polymer-rich and a water-rich (polymer-poor) phase, followed by the formation of dense polymer assemblies. The size and shape of the self-assembled structures are in consistence with the results obtained by RAFT polymerization of HPMA in the presence of GMA−thiocarbonylthio macroCTA. Besides the nucleation and growth of the molecular self-assemblies, coalescence/fusion of the self-assemblies is also observed. Arising from unique features of the graphene layer (impermeability to small molecules, flexibility, and excellent thermal and electrical conductivity), GLC can extend the LC-TEM application in imaging organic/soft matter by enhancing image contrast and mitigating electron-beam-induced damage.

■ ASSOCIATED CONTENT

Supporting Information

The Supporting Information is available free of charge at https://pubs.acs.org/doi/10.1021/acs.macromol.2c02318.

^{1}H NMR spectrum of CDPA, PolyGMA macroCTA, time-dependent RAFT polymerization, GMA and HPMA copolymerization, schematic illustrations for UV-light-induced and electron-beam-induced RAFT copolymerization, DLS traces and particle size analysis of PolyGMA-*b*-PolyHPMA assemblies, TEM images for EELS spectra of the polymer solution, TEM images of PolyGMA-*b*-PolyHMPA control experiments, compound structures, and micelle dissolution (PDF)

Movie S1: bubble formation in GLC during TEM imaging (MP4)

Movie S2: polymerization-induced self-assembly of PolyGMA-*b*-PolyHPMA block copolymer micelles from HPMA monomer solution analyzed by GLC-TEM at an electron dose of ∼1.2 $e^-/(Å^2\ s)$ (MP4)

Movie S3: polymerization-induced self-assembly of PolyGMA-*b*-PolyHPMA block copolymer from HPMA monomer solution analyzed by GLC-TEM at an electron dose of ∼0.8 $e^-/(Å^2\ s)$ (MP4)

Movie S4: GLC-TEM imaging of a solution containing only PolyGMA macroCTA in water (MP4)

Movie S5: GLC-TEM imaging of a solution containing only HPMA in water (MP4)

Movie S6: dissolution of a PolyGMA-*b*-PolyHPMA micelle during GLC-TEM experiment (MP4)

■ AUTHOR INFORMATION

Corresponding Author

Reza Shahbazian-Yassar − *Department of Biomedical Engineering, University of Illinois at Chicago, Chicago, Illinois 60607, United States;* orcid.org/0000-0002-7744-4780; Email: rsyassar@uic.edu

Authors

Vahid Jabbari − *Department of Biomedical Engineering, University of Illinois at Chicago, Chicago, Illinois 60607, United States*

https://doi.org/10.1021/acs.macromol.2c02318
Macromolecules 2023, 56, 3171−3182

Abhijit H. Phakatkar − *Department of Biomedical Engineering, University of Illinois at Chicago, Chicago, Illinois 60607, United States*
Azadeh Amiri − *Department of Biomedical Engineering, University of Illinois at Chicago, Chicago, Illinois 60607, United States*
Alireza Ghorbani − *Department of Biomedical Engineering, University of Illinois at Chicago, Chicago, Illinois 60607, United States*

Complete contact information is available at: https://pubs.acs.org/10.1021/acs.macromol.2c02318

Author Contributions

This study was conceptualized by V.J. and R.S.-Y.; V.J. performed polymer synthesis and characterization, GLC grid preparation and assembly, and preparation of manuscript, figures, and Supporting Information; A.H.P. performed GLC grid preparation and assembly, GLC-TEM experiments, and TEM videos acquisition; A.A. performed image analysis of TEM videos and the quantification of TEM images and contributed to the corresponding discussion; A.G. performed GLC-TEM experiments, TEM videos, and EELS acquisition.

Notes

The authors declare no competing financial interest.

■ ACKNOWLEDGMENTS

R.S.-Y. acknowledges the financial support from the National Science Foundation (NSF 1805938). The authors also acknowledge the Research Resources Center (RRC) at the University of Illinois at Chicago, especially the Director of Electron Microscopy Core, Dr. Fengyuan Shi.

■ REFERENCES

(1) Zubarev, E. R.; Pralle, M. U.; Sone, E. D.; Stupp, S. I. Self-Assembly of Dendron Rodcoil Molecules into Nanoribbons. *J. Am. Chem. Soc.* **2001**, *123* (17), 4105−4106.
(2) Hill, J. P.; Jin, W.; Kosaka, A.; Fukushima, T.; Ichihara, H.; Shimomura, T.; Ito, K.; Hashizume, T.; Ishii, N.; Aida, T. Graphitic Nanotube. *Science* **2004**, *304*, 1481−1483.
(3) Stupp, S. I.; Lebonheur, V.; Walker, K.; Li, L. S.; Huggins, K. E.; Keser, M.; Amstutz, A. Supramolecular Materials: Self-Organized Nanostructures. *Science* **1997**, *276*, 384.
(4) Hirschberg, J. H. K. K.; Brunsveld, L.; Ramzi, A.; Vekemans, J. A. J. M.; Sijbesma, R. P.; Meijer, E. W. Helical Self-Assembled Polymers from Cooperative Stacking of Hydrogen-Bonded Pairs. *Nature* **2000**, *407* (6801), 167−170.
(5) Liu, B.; Cao, Y.; Huang, Z.; Duan, Y.; Che, S. Silica Biomineralization via the Self-Assembly of Helical Biomolecules. *Adv. Mater.* **2015**, *27* (3), 479−497.
(6) Mauro, M.; Aliprandi, A.; Septiadi, D.; Kehr, N. S.; De Cola, L. When Self-Assembly Meets Biology: Luminescent Platinum Complexes for Imaging Applications. *Chem. Soc. Rev.* **2014**, *43* (12), 4144−4166.
(7) Wang, L.; Wu, A.; Wei, G. Graphene-Based Aptasensors: From Molecule-Interface Interactions to Sensor Design and Biomedical Diagnostics. *Analyst* **2018**, *143* (7), 1526−1543.
(8) Wang, L.; Zhang, Y.; Wu, A.; Wei, G. Designed Graphene-Peptide Nanocomposites for Biosensor Applications: A Review. *Anal. Chim. Acta* **2017**, *985*, 24−40.
(9) Discher, B. M.; Won, Y. Y.; Ege, D. S.; Lee, J. C. M.; Bates, F. S.; Discher, D. E.; Hammer, D. A. Polymersomes: Tough Vesicles Made from Diblock Copolymers. *Science (80-.)* **1999**, *284* (5417), 1143−1146.
(10) Holder, S. J.; Sommerdijk, N. A. J. M. New Micellar Morphologies from Amphiphilic Block Copolymers: Disks, Toroids and Bicontinuous Micelles. *Polym. Chem.* **2011**, *2* (5), 1018−1028.
(11) Du, J. Polymer Vesicles. *Adv. Hierarchical Nanostructured Mater.* **2014**, 177−192.
(12) Whitesides, G. M.; Grzybowski, B. Self-Assembly at All Scales. *Science (80-.)* **2002**, *295* (5564), 2418−2421.
(13) Patterson, J. P.; Robin, M. P.; Chassenieux, C.; Colombani, O.; O'Reilly, R. K. The Analysis of Solution Self-Assembled Polymeric Nanomaterials. *Chem. Soc. Rev.* **2014**, *43* (8), 2412−2425.
(14) Figg, C. A.; Simula, A.; Gebre, K. A.; Tucker, B. S.; Haddleton, D. M.; Sumerlin, B. S. Polymerization-Induced Thermal Self-Assembly (PITSA). *Chem. Sci.* **2015**, *6* (2), 1230−1236.
(15) Wan, W. M.; Sun, X. L.; Pan, C. Y. Morphology Transition in RAFT Polymerization for Formation of Vesicular Morphologies in One Pot. *Macromolecules* **2009**, *42* (14), 4950−4952.
(16) Li, C.; Tho, C. C.; Galaktionova, D.; Chen, X.; Král, P.; Mirsaidov, U. Dynamics of Amphiphilic Block Copolymers in an Aqueous Solution: Direct Imaging of Micelle Formation and Nanoparticle Encapsulation. *Nanoscale* **2019**, *11* (5), 2299−2305.
(17) Touve, M. A.; Wright, D. B.; Mu, C.; Sun, H.; Park, C.; Gianneschi, N. C. Block Copolymer Amphiphile Phase Diagrams by High-Throughput Transmission Electron Microscopy. *Macromolecules* **2019**, *52* (15), 5529−5537.
(18) Nagamanasa, K. H.; Wang, H.; Granick, S. Liquid-Cell Electron Microscopy of Adsorbed Polymers. *Adv. Mater.* **2017**, *29* (41), 1−6.
(19) Li, C.; Tho, C. C.; Galaktionova, D.; Chen, X.; Král, P.; Mirsaidov, U. Dynamics of Amphiphilic Block Copolymers in an Aqueous Solution: Direct Imaging of Micelle Formation and Nanoparticle Encapsulation. *Nanoscale* **2019**, *11* (5), 2299−2305.
(20) Smith, B. J.; Parent, L. R.; Overholts, A. C.; Beaucage, P. A.; Bisbey, R. P.; Chavez, A. D.; Hwang, N.; Park, C.; Evans, A. M.; Gianneschi, N. C.; Dichtel, W. R. Colloidal Covalent Organic Frameworks. *ACS Cent. Sci.* **2017**, *3* (1), 58−65.
(21) Woehl, T. J.; Evans, J. E.; Arslan, I.; Ristenpart, W. D.; Browning, N. D. Direct in Situ Determination of the Mechanisms Controlling Nanoparticle Nucleation and Growth. *ACS Nano* **2012**, *6* (10), 8599−8610.
(22) Williamson, M. J.; Tromp, R. M.; Vereecken, P. M.; Hull, R.; Ross, F. M. Dynamic Microscopy of Nanoscale Cluster Growth at the Solid-Liquid Interface. *Nat. Mater.* **2003**, *2* (8), 532−536.
(23) Patterson, J. P.; Abellan, P.; Denny, M. S.; Park, C.; Browning, N. D.; Cohen, S. M.; Evans, J. E.; Gianneschi, N. C. Observing the Growth of Metal-Organic Frameworks by in Situ Liquid Cell Transmission Electron Microscopy. *J. Am. Chem. Soc.* **2015**, *137* (23), 7322−7328.
(24) Parent, L. R.; Gnanasekaran, K.; Korpanty, J.; Gianneschi, N. C. 100th Anniversary of Macromolecular Science Viewpoint: Polymeric Materials by in Situ Liquid-Phase Transmission Electron Microscopy. *ACS Macro Lett.* **2021**, *10* (1), 14−38.
(25) Bae, Y.; Ha, M. Y.; Bang, K. T.; Yang, S.; Kang, S. Y.; Kim, J.; Sung, J.; Kang, S.; Kang, D.; Lee, W. B.; Choi, T. L.; Park, J. Conformation Dynamics of Single Polymer Strands in Solution. *Adv. Mater.* **2022**, *34* (32), 1−8.
(26) Touve, M. A.; Figg, C. A.; Wright, D. B.; Park, C.; Cantlon, J.; Sumerlin, B. S.; Gianneschi, N. C. Polymerization-Induced Self-Assembly of Micelles Observed by Liquid Cell Transmission Electron Microscopy. *ACS Cent. Sci.* **2018**, *4* (5), 543−547.
(27) Evans, J. E.; Jungjohann, K. L.; Wong, P. C. K.; Chiu, P. L.; Dutrow, G. H.; Arslan, I.; Browning, N. D. Visualizing Macromolecular Complexes with in Situ Liquid Scanning Transmission Electron Microscopy. *Micron* **2012**, *43* (11), 1085−1090.
(28) Yamazaki, T.; Kimura, Y.; Vekilov, P. G.; Furukawa, E.; Shirai, M.; Matsumoto, H.; Van Driessche, A. E. S.; Tsukamoto, K. Two Types of Amorphous Protein Particles Facilitate Crystal Nucleation. *Proc. Natl. Acad. Sci. U. S. A.* **2017**, *114* (9), 2154−2159.
(29) Smeets, P. J. M.; Cho, K. R.; Kempen, R. G. E.; Sommerdijk, N. A. J. M.; De Yoreo, J. J. Calcium Carbonate Nucleation Driven by Ion

Binding in a Biomimetic Matrix Revealed by in Situ Electron Microscopy. *Nat. Mater.* **2015**, *14* (4), 394−399.
(30) Proetto, M. T.; Rush, A. M.; Chien, M. P.; Abellan Baeza, P.; Patterson, J. P.; Thompson, M. P.; Olson, N. H.; Moore, C. E.; Rheingold, A. L.; Andolina, C.; Millstone, J.; Howell, S. B.; Browning, N. D.; Evans, J. E.; Gianneschi, N. C. Dynamics of Soft Nanomaterials Captured by Transmission Electron Microscopy in Liquid Water. *J. Am. Chem. Soc.* **2014**, *136* (4), 1162−1165.
(31) Hoppe, S. M.; Sasaki, D. Y.; Kinghorn, A. N.; Hattar, K. In-Situ Transmission Electron Microscopy of Liposomes in an Aqueous Environment. *Langmuir* **2013**, *29* (32), 9958−9961.
(32) Ianiro, A.; Wu, H.; van Rijt, M. M. J.; Vena, M. P.; Keizer, A. D. A.; Esteves, A. C. C.; Tuinier, R.; Friedrich, H.; Sommerdijk, N. A. J. M.; Patterson, J. P. Liquid−Liquid Phase Separation during Amphiphilic Self-Assembly. *Nat. Chem.* **2019**, *11* (4), 320−328.
(33) Gnanasekaran, K.; Chang, H.; Smeets, P. J. M.; Korpanty, J.; Geiger, F. M.; Gianneschi, N. C. In Situ Ni2+Stain for Liposome Imaging by Liquid-Cell Transmission Electron Microscopy. *Nano Lett.* **2020**, *20* (6), 4292−4297.
(34) Gnanasekaran, K.; Korpanty, J.; Berger, O.; Hampu, N.; Halperin-Sternfeld, M.; Cohen-Gerassi, D.; Adler-Abramovich, L.; Gianneschi, N. C. Dipeptide Nanostructure Assembly and Dynamics via in Situ Liquid-Phase Electron Microscopy. *ACS Nano* **2021**, *15* (10), 16542−16551.
(35) Korpanty, J.; Parent, L. R.; Hampu, N.; Weigand, S.; Gianneschi, N. C. Thermoresponsive Polymer Assemblies via Variable Temperature Liquid-Phase Transmission Electron Microscopy and Small Angle X-Ray Scattering. *Nat. Commun.* **2021**, DOI: 10.1038/s41467-021-26773-z.
(36) Korpanty, J.; Gnanasekaran, K.; Venkatramani, C.; Zang, N.; Gianneschi, N. C. Organic Solution-Phase Transmission Electron Microscopy of Copolymer Nanoassembly Morphology and Dynamics. *Cell Reports Phys. Sci.* **2022**, *3* (3), 100772.
(37) Rizvi, A.; Mulvey, J. T.; Carpenter, B. P.; Talosig, R.; Patterson, J. P. A Close Look at Molecular Self-Assembly with the Transmission Electron Microscope. *Chem. Rev.* **2021**, *121* (22), 14232−14280.
(38) Early, J. T.; Yager, K. G.; Lodge, T. P. Direct Observation of Micelle Fragmentation via in Situ Liquid-Phase Transmission Electron Microscopy. *ACS Macro Lett.* **2020**, *9* (5), 756−761.
(39) Rizvi, A.; Mulvey, J. T.; Patterson, J. P. Observation of Liquid−Liquid-Phase Separation and Vesicle Spreading during Supported Bilayer Formation via Liquid-Phase Transmission Electron Microscopy. *Nano Lett.* **2021**, *21* (24), 10325−10332.
(40) Subramanian, V.; Martin, D. C. In Situ Observations of Nanofibril Nucleation and Growth during the Electrochemical Polymerization of Poly(3,4-Ethylenedioxythiophene) Using Liquid-Phase Transmission Electron Microscopy. *Nano Lett.* **2021**, *21* (21), 9077−9084.
(41) Alam, S. B.; Soligno, G.; Yang, J.; Bustillo, K. C.; Ercius, P.; Zheng, H.; Whitelam, S.; Chan, E. M. Dynamics of Polymer Nanocapsule Buckling and Collapse Revealed by In Situ Liquid-Phase TEM. *Langmuir* **2022**, *38* (23), 7168−7178.
(42) Isaacson, K. J.; Van Devener, B. R.; Steinhauff, D. B.; Jensen, M. M.; Cappello, J.; Ghandehari, H. Liquid-Cell Transmission Electron Microscopy for Imaging of Thermosensitive Recombinant Polymers. *J. Controlled Release* **2022**, *344*, 39−49.
(43) Yuk, J. M.; Park, J.; Ercius, P.; Kim, K.; Hellebusch, D. J.; Crommie, M. F.; Lee, J. Y.; Zettl, A.; Alivisatos, A. P. High-Resolution EM of Colloidal Nanocrystal Growth Using Graphene Liquid Cells. *Science* **2012**, *336* (6077), 61−64.
(44) Loh, N. D.; Sen, S.; Bosman, M.; Tan, S. F.; Zhong, J.; Nijhuis, C. A.; Král, P.; Matsudaira, P.; Mirsaidov, U. Multistep Nucleation of Nanocrystals in Aqueous Solution. *Nat. Chem.* **2017**, *9* (1), 77−82.
(45) Powers, A. S.; Liao, H.-G.; Raja, S. N.; Bronstein, N. D.; Alivisatos, A. P.; Zheng, H. Tracking Nanoparticle Diffusion and Interaction during Self-Assembly in a Liquid Cell. *Nano Lett.* **2017**, *17* (1), 15−20.
(46) Král, P. *Unveiling Growth and Dynamics of Liposomes by Graphene Liquid Cell-Transmission Electron Microscopy*, 2023.
(47) Zhang, Q.; Hong, J. D.; Hoogenboom, R. A Triple Thermoresponsive Schizophrenic Diblock Copolymer. *Polym. Chem.* **2013**, *4* (16), 4322−4325.
(48) Figg, C. A.; Carmean, R. N.; Bentz, K. C.; Mukherjee, S.; Savin, D. A.; Sumerlin, B. S. Tuning Hydrophobicity To Program Block Copolymer Assemblies from the Inside Out. *Macromolecules* **2017**, *50* (3), 935−943.
(49) Wang, X.; Figg, C. A.; Lv, X.; Yang, Y.; Sumerlin, B. S.; An, Z. Star Architecture Promoting Morphological Transitions during Polymerization-Induced Self-Assembly. *ACS Macro Lett.* **2017**, *6* (4), 337−342.
(50) Cunningham, V. J.; Alswieleh, A. M.; Thompson, K. L.; Williams, M.; Leggett, G. J.; Armes, S. P.; Hill, B.; Yorkshire, S. Poly(Glycerol Monomethacrylate)−Poly(Benzyl Methacrylate) SI.Pdf, pp 1−4.
(51) Li, Z.; Chen, C.; Gröger, S.; Kressler, J. Detection of Chirality of Poly(Glycerol Methacrylate)s after Derivatization by 1H NMR Spectroscopy. *Polymer (Guildf).* **2012**, *53* (13), 2613−2618.
(52) Wan, W. M.; Pan, C. Y. One-Pot Synthesis of Polymeric Nanomaterials via RAFT Dispersion Polymerization Induced Self-Assembly and Re-Organization. *Polym. Chem.* **2010**, *1* (9), 1475−1484.
(53) He, W. D.; Sun, X. L.; Wan, W. M.; Pan, C. Y. Multiple Morphologies of PAA-b-PSt Assemblies throughout RAFT Dispersion Polymerization of Styrene with PAA Macro-CTA. *Macromolecules* **2011**, *44* (9), 3358−3365.
(54) Li, Y.; Armes, S. P. RAFT Synthesis of Sterically Stabilized Methacrylic Nanolatexes and Vesicles by Aqueous Dispersion Polymerization. *Angew. Chemie - Int. Ed.* **2010**, *49* (24), 4042−4046.
(55) Huang, C. Q.; Pan, C. Y. Direct Preparation of Vesicles from One-Pot RAFT Dispersion Polymerization. *Polymer (Guildf).* **2010**, *51* (22), 5115−5121.
(56) Cai, W.; Wan, W.; Hong, C.; Huang, C.; Pan, C. Morphology Transitions in RAFT Polymerization. *Soft Matter* **2010**, *6* (21), 5554−5561.
(57) Alahmari, F.; Davaasuren, B.; Emwas, A. H.; Costa, P. M. F. J.; Rothenberger, A. Tris(Ethylenediamine)Nickel(II) Thio-Hydroxo-germanate Monohydrate: Synthesis, Crystal Structure, 1H NMR, EPR, Optical and Magnetic Properties. *Inorg. Chim. Acta* **2019**, *488*, 145−151.
(58) Pell, A. J.; Pintacuda, G.; Grey, C. P. Paramagnetic NMR in Solution and the Solid State. *Prog. Nucl. Magn. Reson. Spectrosc.* **2019**, *111*, 1−271.
(59) Touve, M. A.; Figg, C. A.; Wright, D. B.; Park, C.; Cantlon, J.; Sumerlin, B. S.; Gianneschi, N. C. Polymerization-Induced Self-Assembly of Micelles Observed by Liquid Cell Transmission Electron Microscopy. *ACS Cent. Sci.* **2018**, *4* (5), 543−547.
(60) Keskin, S.; Pawell, C.; de Jonge, N. Verification of Water Presence in Graphene Liquid Cells. *Micron* **2021**, *149*, 103109.
(61) Ghodsi, S. M.; Anand, S.; Shahbazian-Yassar, R.; Shokuhfar, T.; Megaridis, C. M. In Situ Study of Molecular Structure of Water and Ice Entrapped in Graphene Nanovessels. *ACS Nano* **2019**, *13* (4), 4677−4685.
(62) Firlar, E.; Ouy, M.; Covnot, L.; Xing, Y.; Lee, D.; Chan, A.; He, Y.; Song, B.; Afelik, S.; Wang, Y.; Shahbazian-Yassar, R.; Oberholzer, J.; Shokuhfar, T. In Situ Graphene Liquid Cell-Transmission Electron Microscopy Study of Insulin Secretion in Pancreatic Islet Cells. *Int. J. Nanomedicine* **2019**, *14*, 371−382.
(63) Parent, L. R.; Bakalis, E.; Ramírez-Hernández, A.; Kammeyer, J. K.; Park, C.; De Pablo, J.; Zerbetto, F.; Patterson, J. P.; Gianneschi, N. C. Directly Observing Micelle Fusion and Growth in Solution by Liquid-Cell Transmission Electron Microscopy. *J. Am. Chem. Soc.* **2017**, *139* (47), 17140−17151.
(64) Woehl, T. J.; Abellan, P. Defining the Radiation Chemistry during Liquid Cell Electron Microscopy to Enable Visualization of Nanomaterial Growth and Degradation Dynamics. *J. Microsc.* **2017**, *265* (2), 135−147.
(65) Schneider, N. M.; Norton, M. M.; Mendel, B. J.; Grogan, J. M.; Ross, F. M.; Bau, H. H. Electron-Water Interactions and Implications

for Liquid Cell Electron Microscopy. *J. Phys. Chem. C* **2014**, *118* (38), 22373−22382.
(66) Lund, R.; Willner, L.; Monkenbusch, M.; Panine, P.; Narayanan, T.; Colmenero, J.; Richter, D. Structural Observation and Kinetic Pathway in the Formation of Polymeric Micelles. *Phys. Rev. Lett.* **2009**, *102* (18), 1−4.
(67) Choi, Y.; Kang, S.; Lim, S.; Kim, W.; Kim, J. R.; Lee, J. H.; An, K. Quasieigenstate Coalescence in an Atom-Cavity Quantum Composite. *Phys. Rev. Lett.* **2010**, *104* (15), 16−19.
(68) Jensen, G. V.; Lund, R.; Gummel, J.; Narayanan, T.; Pedersen, J. S. Monitoring the Transition from Spherical to Polymer-like Surfactant Micelles Using Small-Angle X-Ray Scattering. *Angew. Chemie - Int. Ed.* **2014**, *53* (43), 11524−11528.
(69) Nyrkova, I. A.; Semenov, A. N. On the Theory of Micellization Kinetics. *Macromol. Theory Simulations* **2005**, *14* (9), 569−585.
(70) Halperin, A.; Alexander, S. Polymeric Micelles: Their Relaxation Kinetics. *Macromolecules* **1989**, *22* (5), 2403−2412.
(71) Gummel, J.; Sztucki, M.; Narayanan, T.; Gradzielski, M. Concentration Dependent Pathways in Spontaneous Self-Assembly of Unilamellar Vesicles. *Soft Matter* **2011**, *7* (12), 5731−5738.
(72) Blanazs, A.; Madsen, J.; Battaglia, G.; Ryan, A. J.; Armes, S. P. Mechanistic Insights for Block Copolymer Morphologies: How Do Worms Form Vesicles? *J. Am. Chem. Soc.* **2011**, *133* (41), 16581−16587.
(73) Shen, H.; Zhang, L.; Eisenberg, A. Thermodynamics of Crew-Cut Micelle Formation of Polystyrene-b-Poly(Acrylic Acid) Diblock Copolymers in DMF/H_2O Mixtures. *J. Phys. Chem. B* **1997**, *101* (24), 4697−4708.
(74) Yu, Y.; Eisenberg, A. Control of Morphology through Polymer-Solvent Interactions in Crew-Cut Aggregates of Amphiphilic Block Copolymers. *J. Am. Chem. Soc.* **1997**, *119* (35), 8383−8384.
(75) Zheng, G.; Pan, C. Reversible Addition-Fragmentation Transfer Polymerization in Nanosized Micelles Formed in Situ. *Macromolecules* **2006**, *39* (1), 95−102.
(76) Nicolai, T.; Colombani, O.; Chassenieux, C. Dynamic Polymeric Micelles versus Frozen Nanoparticles Formed by Block Copolymers. *Soft Matter* **2010**, *6* (14), 3111−3118.
(77) Jiang, N. Note on in Situ (Scanning) Transmission Electron Microscopy Study of Liquid Samples. *Ultramicroscopy* **2017**, *179*, 81−83.
(78) Parent, L. R.; Robinson, D. B.; Woehl, T. J.; Ristenpart, W. D.; Evans, J. E.; Browning, N. D.; Arslan, I. Direct in Situ Observation of Nanoparticle Synthesis in a Liquid Crystal Surfactant Template. *ACS Nano* **2012**, *6* (4), 3589−3596.
(79) Abellan, P.; Woehl, T. J.; Parent, L. R.; Browning, N. D.; Evans, J. E.; Arslan, I. Factors Influencing Quantitative Liquid (Scanning) Transmission Electron Microscopy. *Chem. Commun.* **2014**, *50* (38), 4873−4880.

NOTE ADDED AFTER ASAP PUBLICATION

This paper was published ASAP on April 11, 2023, with the PDF Supporting Information file incorrectly linked to a movie file. The corrected version was reposted on April 14, 2023.

https://doi.org/10.1021/acs.macromol.2c02318
Macromolecules 2023, 56, 3171−3182